Thesis Proposal

submitted for the degree of

Doctor of Philosophy in Mechanical Engineering

Entitled

Design of Hybrid Lattice Support Structures Considering Practical Additive Manufacturing Constraints

Date of Submission: June 28th, 2023

Submitted by:	Lisha White
Advisors:	Dr. Jonathan Cagan (Chair), Carnegie Mellon University
	Dr. Yongjie Jessica Zhang (Chair), Carnegie Mellon University
Committee Members:	Dr. Anthony Rollett, Carnegie Mellon University
	Dr. Guanglu Zhang, Carnegie Mellon University

Abstract

Support structure design is imperative in the design of additively manufactured parts with overhang features in the build direction, especially those fabricated using laser powder bed fusion (LPBF). When designed effectively, support structures quickly dissipate heat and mitigate part distortion without driving up excessive costs. Lattices, composed of individual unit cells strategically arranged to achieve a desired function, are a promising solution as a support structure. Prior research has designed these structures utilizing both gradient- and non-gradient-based optimizers; however, there still exist limitations within current work. Gradient-based optimizers pose challenges regarding limited design exploration and non-differentiable design variables. Non-gradient-based optimizers, proven to be an effective alternative solution, are known to be too slow in comparison to gradient-based optimizers and have not yet been applied to consider the multi-physics functionality of support structure. Thus, to improve the current state of the design of support structures, we propose a robust framework that facilitates the design of lattice support structures.

Towards the development of this new framework, preliminary work has been performed to investigate the design opportunities and apply multi-functional support structure properties within practical timespans. Correspondingly, the work executed in this proposal demonstrates how implementing homogenization approximation techniques, stage-dependent actions, and stochastic optimization can be employed to maximize heat dissipation for lattice support structures. Non-gradient-based simulated annealing optimization is utilized to quickly optimize the distribution of a library comprised of commonly employed unit cells while adhering to user-defined manufacturing constraints. The utilization of stage-dependent actions and homogenization approximation with SA is shown to provide a broader exploration of the design space without excessive computation time for multiple scales. The current framework is validated through the case study of a cantilever beam and shows promising results for the case study of an aerospace bracket. Within each case study, consistently obtained increased heat dissipation is accomplished compared to the uniformly distributed benchmark design while still satisfying manufacturing constraints. We seek to expand the functionality of the current framework to include a methodology for new materials and asymmetric, curved structures. Moreover, by optimizing support for real components, further confirmation of the practicality of the proposed work will be provided. To ensure comparable results, it is intended for the optimizer and simulations to be calibrated to match the residual deformation of experimental results prior to optimization. The proposed framework will enable designers to manufacture complex geometries with customizable support structure properties. It will also advance the current research within a range of disciplines, including design, optimization, and AM of lattices.

Contents

1. Introduction and Motivation 4

1.1. Broader Impacts 4

1.2. Related Work and Existing Needs 5

1.2.1. Existing Gradient-Based Optimizers 5

1.2.2. Existing Non-Gradient-Based Optimizers 6

1.2.3. Motivation 6

1.3. Thesis Statement 6

2. Research Overview 7

2.1. Objective 1: Coupling Simulated Annealing and Homogenization to Design Thermally Conductive Hybrid Lattice Support Structures for LPBF 7

2.2. Objective 2: Designing Thermally Conductive Hybrid Lattice Support Structures Constrained by Residual Stress and Deformation for LPBF 7

2.3. Objective 3: Extending Lattice Support Structure Design to Curved Interfaces 7

3. Past Work 7

3.1. Objective 1 7

Objective 1.1: Coupling stochastic optimization and homogenization approximation to maximize heat dissipation with manufacturing constraints in LPBF 8

Objective 1.2: Constructing expedited evaluation approaches for non-gradient-based optimizers to obtain the optimal combination of lattice structures. 9

4. Current Work 12

4.1. Objective 2 12

Objective 2.1: Formulating the optimization problem to maximize heat dissipation while considering structural constraints 12

Objective 2.2: Predicting both thermal and structural properties of lattice support structures for expedited evaluation using homogenization approximation 15

4.2. Objective 3 18

Objective 3.1: Generating results for inherent strain inputs for arbitrary materials 19

Objective 3.2: Incorporating complex structures into lattice support structure design framework 19

Objective 3.3: Validating the framework through experimental components. 20

Expected Contributions 20

4.3. Timeline 20

5. Intellectual Merit 21

6. Acknowledgements 22

7. References 22

1. Introduction and Motivation

Additive manufacturing (AM) is a rapidly expanding industrial field due to its ability to create customizable, complex structures [1]. Laser Powder Bed Fusion (LPBF) is a popular approach in the creation of metal parts within AM. This approach has been repeatedly proven to create structures such as topology-optimized structures for reduced weight and components with internal channels. To create such intricate features, a concentrated, high-energy heat source fuses metal powder layers within solid metal layers in the desired cross-section [1,2]. After each layer is spread, melted, and solidified, another layer of powder is added and the process is repeated until the final part is created. Support structures are imperative when manufacturing parts with overhangs, downward facing surfaces greater than 5mm in length [3,4]. Two main functions of the support structure are to transfer heat and anchor the part to the base plate [3–6]. Therefore, poor design of these structures will lead to part inaccuracy and may damage the machine, both factors which will significantly increase the cost to manufacture. Much effort has been devoted to identifying a generalizable set of guidelines designers should consider when manufacturing within AM, particularly LPBF. Despite the efforts, it can be difficult to include when designing structures manually when some of the design rules have trade-offs such as high stiffness but low weight [7]. To automate this design procedure, one question arises: **what is an efficient approach designers can employ for the generation of support structures that adhere to AM constraints?**

Researchers have introduced approaches to generate support structures by using combinations of unit cells to create lattices [1–4]. The self-supporting unit cells are strategically designed on a microscopic scale and distributed within the design domain to achieve a macroscopic property. Within support structure design, the lattice support structures are typically optimized with the main objective to either dissipate heat or minimize compliance of the part. Optimization approaches previously proposed typically frame the problem in a continuous domain by either redistributing material in the design domain or of a unit cell that is periodic using gradient-based optimization techniques [6,8–10]. In doing so, challenges regarding non-differentiable design variables and limited design exploration emerge. Non-gradient-based optimization is a possible solution [11,12] but the approach is comparably slow compared to gradient-based optimizers and has not been applied to the thermal requirements for support structures. To fully exploit the opportunities non-gradient-based optimizers possess, **what modifications can be made to existing optimization approaches for application to design lattice support structures?**

To address these questions for support structure design, we propose a framework to utilize a modified, non-gradient-based optimizer to generate support structures that adhere to multiple AM constraints without excessive computational time. This goal can be achieved within a three-part procedure. We will (1) establish a preliminary framework to create a hybrid lattice support structure with the aim to dissipate heat with user-defined constraints for simple structures, (2) apply constraints that capture both the thermal and mechanical response, and (3) validate the approach with experimental results. My research will provide the necessary process for advancing the current state-of-the-art methods to produce printable lattice designs and support structures for AM.

1.1. Broader Impacts

This project studies the fabrication of support structures but the methods proposed can be applied to a range of disciplines pertaining to manufacturing and optimization. It directly contributes to the research area of advanced AM as it considers design objectives and constraints. The ability to design structures with multifunctionality without experimental trials is imperative to saving costs. By creating models to simulate the manufacturing process, the multi-physics properties of the design can be predicted within hours and changed before any experiments are performed. The proposed work can also provide a new approach to reframing continuous problems into integer problems that can be solved in a more efficient manner, particularly those that rely on finite element methods (FEM).

AM has simplified the manufacturing of lattice structures, particularly for lightweight design [1,7,13,14]; therefore, having a robust and efficient approach to design these structures would broaden their application. In this project, the aim is to design the lattice as a support structure that can be manufacturable using LPBF. This application can lead to expanded research activities on efficient and economic design of support structures based on numerical computational methods and attracts further investigations to design different types of lattice support structures based on practical manufacturing requirements and performance.

1.2. Related Work and Existing Needs

In part due to the non-uniform application of heat and the steep thermal gradient caused by the concentrated, high-power energy source, components manufactured using LPBF may have undesirable shapes and aesthetics when not designed correctly. The non-uniform distribution will result in distortions [8,10,15–17], discoloration [18], high surface roughness in the final part [2,19,20], and could damage the machine due to collision between the part and the powder recoater [2,21–23]. These deformities may be mitigated by redesigning the configuration within the build chamber or even the component itself; however, this cannot always be achieved. Therefore, support material is required. Support structures within LPBF are employed to both anchor the part to the build plate and to help dissipate heat [3–6]. For large overhangs, the low thermal conductivity of the powder and the non-uniform heat distribution, caused by the high energy source, will cause heat to accumulate in various locations. This will result in distortions, discoloration, and high surface roughness in the final part.

One approach to generating support structure is to create lattices as opposed to redistributing the material within the entire design domain, generally referred to as topology optimization. Lattices are composed of self-supporting mesoscopic unit cells that are microscopically designed and macroscopically distributed throughout the structure [3,6,10,17]. When used as support structures, they have been proven to dissipate heat [6,8] and minimize residual distortion [10] within parts. However, the procedure to design these macroscopic structures has yet to be fully exploited due to the current methods within gradient- and non-gradient-based optimization. Gradient-based optimizers find a solution to satisfy the objective and user-defined constraints by differentiating the design variables. They are known for their ability to propose fast solutions; however, these solutions are subject to getting stuck in the local optima. Additionally, the entire basis of gradient-based optimization requires differentiable components (i.e., design variables), which can be difficult to derive [8]. Non-gradient-based optimizers do not use derivatives to find the solution. They have been proposed as alternatives to gradient-based optimizers, but they are typically more time-consuming when proposing a solution. Research regarding both the gradient-based and non-gradient-based approaches to creating lattice support structures is summarized in this section.

1.2.1. **Existing Gradient-Based Optimizers**

Prior research has applied existing gradient-based optimization methods to create lattice support structures. One approach is to apply topology optimization to a single unit cell that is periodically repeated. By discretizing a single unit cell into elements, the design variables are the materials labeled 0/1 (i.e., void/material) [24]. This method assigns a continuous density value between 0 and 1 to avoid binary values, allowing for the use of gradient-based optimizers. This methodology was shown to be able to create a lattice support structure with better dissipation of heat than the traditional tree-like support structures and pins [6]. However, one major problem with a single periodic unit cell is that it does not consider the inherent spatial non-uniformity of the LPBF process. By not considering the heterogeneity of the transfer of heat, for example, unnecessarily excessive amounts of material will be incorporated into the design yielding increased material waste.

Another approach is to discretize the entire domain with coarse elements that are represented as individual unit cells with an assigned density [8]. By utilizing a library composed of predefined material properties, this approach allows designers to create spatially and temporally dependent lattice structures. Evaluation of the macroscale lattice is accelerated by coupling the library composed of the relative densities of a simple cubic structure's effective properties with the homogenization approximation, which instead employs a representative volume element (RVE) [8,10,23,25–29]. This drastically reduces the number of design variables from microscale material elements to mesoscale unit cells to choose for each possible location [8,10,25,30]. By utilizing a gradient-based optimization method, the model was able to reduce the liquid lifetime (i.e., the amount of time the top layer is above liquid temperature) yielding reduced residual stress deformation by 42% when compared to the benchmark of a uniformly sized simple cubic lattice support structure. However, only a simple cubic unit cell was optimized for the density, limiting the optimizer's ability to consider more AM constraints, such as post-processing. In addition, the sensitivity analysis, used to guide the optimizer to a local minimum, requires additional approximation due to the transient objective function. For more complex shapes, the accumulated errors resulting from the many approximations can lead to suboptimal results caused by inaccurate sensitivity analysis results. Furthermore, although this was effective for a twin cantilever beam with two planes of symmetry, for more complex, asymmetric structures, the approach may not be able to achieve such success and accuracy.

1.2.2. **Existing Non-Gradient-Based Optimizers**

Non-gradient-based optimizers have been studied as an alternative to gradient-based optimizers as they are not reliant on differentiable design variables. This allows designers to optimize a larger variety of objectives and the ability to explore a larger design space with a reduced chance of being trapped in a local optimum. Two notable non-gradient-based optimizers are genetic algorithms (GAs) and simulated annealing (SA)[31–33]. Between these two optimizers, GAs have been employed to optimize lattices. By following heuristics analogous to Darwinian evolution, GAs generate a population of results that are evaluated in parallel [11,12,27]. When applying GAs to the generation of lattices, another approach to combat the high computational cost associated with the many iterations, researchers have studied the use of homogenization approximation approach [27]. With the predefined library of lattice properties that are simplified into RVEs, this approach has been used to minimize the compliance of triangular struts for a planar lattice design. However, when scaling the model to 3D, computation time will increase drastically. The homogenization approximation may help with reducing the design variables [8] but that will reduce population size and could lead to premature convergence as a result[34].

In opposition to using GAs, SAs do not have the problem of premature convergence as it evaluates one generated state (population of 1 result) per iteration. It has been applied to heat transfer problems to find the optimally directed configuration of a finite number of components [31,35,36]. SA is analogous to the annealing of metal from a high-energy state (i.e., molten) to a low-energy state (i.e., solid) [37]. For each iteration in SA, the energy state (i.e., objective function) of the design is evaluated and compared to the previous state. If the proposed design is better than the previous state, it is accepted as the current state. Otherwise, the acceptance of the proposed state is determined by probability. This is advantageous as it allows for the optimizer to move out of a potential local minimum, even at later stages. One major challenge in utilizing SA for lattice structure design is the computational time required to explore the design space. For traditional SA algorithms, only small perturbations are made within the design space per evaluation iteration [37]. When designing a lattice with hundreds of design variables, the small perturbations per iteration limit the region of exploration at higher annealing temperatures. Therefore, the traditional SA needs to be modified to efficiently explore the design space for lattice structure designs of multiple scales.

1.2.3. **Motivation**

Overhang features for LPBF require support structure to dissipate heat from unsupported regions and to stabilize the structure due to the accumulation of residual stress. Lattice support structures are a promising solution because they are composed of self-supporting unit cells that can be individually tailored and distributed to achieve optimal support structure properties. However, several gaps need to be overcome before lattice support structures can be widely adopted in LPBF design:

1. Restricting types of manufacturable unit cells, such as using a varying density of a simple cubic cell, limits the types of AM constraints that can be considered.
2. Nondifferentiable lattices make it difficult for gradient-based optimizers to fully explore the design space and can lead to inaccuracies due to accumulating approximations.
3. High computation time is a major limitation for using non-gradient-based optimizers, particularly with powerful methods such as SA.

1.3. Thesis Statement

The first aim of this work is to investigate the new design opportunity of lattice support structures fabricated by LPBF by coupling a modified simulated annealing optimizer with homogenization approximation. With the first objective to maximize the dissipation of heat while considering material waste and post-processing, the computational framework is established. Objective 2 broadens the capabilities of the framework by considering structural constraints: residual stress and deformation for horizontal overhang geometries.

The second part of this work attempts to expand on the previously established framework to include structures with inclined and curved overhangs. By exploring three approaches to connect lattice support structures to real parts for printing, it is desired to propose a fully functional framework to automate the optimization of lattice support structures beginning from the selection of a new material.

With these aims, the following thesis statement is proposed:

Lattice support structure design for additive manufacturing (AM) is performed by reframing the optimization problem as a configuration optimization problem to maximize the dissipation of heat while constraining residual stress. By utilizing a modified non-gradient-based optimizer coupled with homogenization approximation to generate support structures, designers can create manufacturable lattice support structures for complex components optimized for the major functionality of support structures of heat dissipation while adhering to AM constraints for practical utilization, including structural integrity.

The underlined portion of the above thesis statement is a statement of intent based on proposed future work. This thesis statement will be edited upon completion of future work to offer more specific insights.

2. Research Overview

To address the need for an efficient framework that considers the design for AM constraints for lattice support structures, we will develop a pipeline demonstrating the utilization of a modified non-gradient-based optimizer. Three major objectives have been identified with corresponding sub-objectives that describe major contributions.

2.1. Objective 1: Coupling Simulated Annealing and Homogenization to Design Thermally Conductive Hybrid Lattice Support Structures for LPBF

Objective 1.1: Coupling stochastic optimization and homogenization approximation to maximize heat dissipation with manufacturing constraints in LPBF

Objective 1.2: Constructing expedited evaluation approaches for non-gradient-based optimizers to obtain optimal combination of lattice structures

2.2. Objective 2: Designing Thermally Conductive Hybrid Lattice Support Structures Constrained by Residual Stress and Deformation for LPBF

Objective 2.1: Formulating the optimization problem to maximize heat dissipation while considering structural constraints
Objective 2.2: Predicting both thermal and structural properties of lattice support structures for expedited evaluation using homogenization approximation

2.3. Objective 3: Extending Lattice Support Structure Design to Curved Interfaces

Objective 3.1: Calibrating simulation results for inherent strain inputs for arbitrary materials
Objective 3.2: Incorporating complex, curved structures for lattice support generation.
Objective 3.3: Validating the framework through experimental components

3. Past Work

3.1. Objective 1: Coupling Simulated Annealing and Homogenization to Design Thermally Conductive Hybrid Lattice Support Structures for LPBF

In this work, a computational framework is introduced to investigate the design opportunity of utilizing non-gradient-based optimization to maximize heat dissipation while adhering to design for AM constraints. The preliminary framework facilitates the design of lattice support structures by coupling the homogenization approximation with stochastic optimization to expedite the iterative evaluation for the objective function. Simulated annealing is utilized to quickly optimize the distribution of three commonly employed unit cells while adhering to user-defined manufacturing constraints. By incorporating both stage-dependent actions and homogenization approximation with the non-gradient optimizer, a broader exploration of the design space is accomplished without compromising computation time. The framework is validated through the case study of a cantilever beam for which optimal hybrid lattice support structures are consistently obtained with about 16% better heat dissipation than the uniformly distributed benchmark design with manufacturing constraints satisfied. Further validation is performed with a transient thermal simulation to obtain the time to reach steady-state temperature.

Objective 1.1: Coupling stochastic optimization and homogenization approximation to maximize heat dissipation with manufacturing constraints in LPBF

The cantilever beam is a commonly used benchmark for the design of support structures and is employed here to introduce this framework, shown in Figure 1. Notably, the framework established in this section is generally applicable to the design of other support structures. When heat is applied to build the cantilever, the lack of support underneath the large overhang results in non-uniform heat distribution and high accumulation of heat [19,20]. As shown in Figure 1, the volume underneath the overhang, the boundary defined by the dashed lines, is denoted as the design domain. By optimizing the distribution of individual unit cells, selected from a library, the heat can transfer from the applied heating to the base plate, located at the bottom plane of the cantilever. In addition, the support structure generated within the design domain must also satisfy multiple user-defined manufacturing constraints.

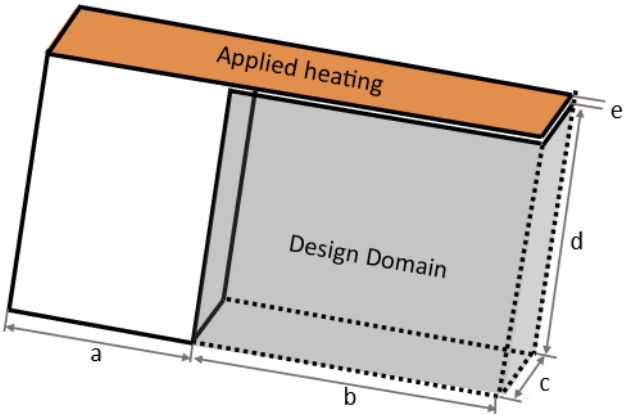

FIGURE 1: Geometry of the cantilever beam (Represented by solid lines) with the design domain (represented by the dashed lines) and variable dimensions.

To begin formulating the optimization problem, the objective function is defined. The metric employed for this study to represent the heat dissipation is the minimization of the heat transfer rate through the base plate, Q_{out}, described in Objective 1.2 and represented as Equation (1). The heat dissipation performance metric, Q_{out}, is chosen here for demonstration purposes as it is a practical measurement as opposed to the commonly employed thermal compliance [38]. Therefore, to minimize Q_{out} is to maximize the dissipation through the system. Other metrics also could be employed in practice based on users' preferences. The optimization problem is formalized as:

$$\begin{aligned} &\text{find} && \mathbf{x} = [x_1, x_2, \ldots, x_n] \text{ to} && \\ &\text{minimize} && Q_{out} = \mathbf{Q}(\mathbf{x}), && (1) \\ &\text{subject to} && \mathbf{KT} = \mathbf{G}, && (2) \\ & && V(\mathbf{x}) < \varepsilon_V * V_{max}, \text{ and} && (3) \\ & && A(\mathbf{x}) < \varepsilon_A * A_{max}, && (4) \end{aligned}$$

where $x_i \in [SC, BV, FC]$, $i \in \{1,2,\ldots,n\}$ and n is the number of geometric design variables. The design domain is evenly discretized to fit the bounding volume of the unit cells; however, the domain can also be partitioned to accommodate design variables with different bounding volumes [39]. The design variables are three commonly employed strut-based unit cells are selected here for the library for demonstration purposes, shown in Figure 3: simple cubic (SC) [8,13,25,26], body-centered vertical strut cubic (BV) [11,40], and face-centered cubic (FC) [13,40,41]. Each self-supporting cell occupies a $2\times2\times2$ mm^3 space. As shown in Table 1, each unit cell has properties that are advantageous to the flow of heat, the volume, or the amount of interfacing area between the part and the unit cell, shown in bold.

Before the optimization procedure can be run, the design domain must be defined. As opposed to a computationally expensive exact solution to heat source input that considers scan pattern and other phenomena associated with the melt pool, the flash method is employed for the layer-by-layer simulation [8,15,42]. To begin the layer-by-layer simulation, the column of height *d* contains all active elements whereas the overhang elements of height *e* are deactivated. For the first heating cycle, a superlayer of elements composed of multiple actual powder layers is activated with a volumetric heat flux at the surface nodes, shown in Figure 2. To calculate the amount of volumetric heat flux, q", the following equation is applied:

$$q'' = (A_b \cdot P)/(d_m \cdot d_s \cdot h), \quad (5)$$

where A_b is the laser absorptivity, P is the power, d_m is the depth of the melt pool, d_s is the spot diameter and h is the hatch space [15]. After heating is applied for a user-defined time, the cooling occurs to simulate the amount of time for the recoater to apply another layer [43]. The cycle of heating and then cooling continues until all overhang element layers have been activated. The base plate is represented as the heat sink and is kept at a constant temperature with an applied convection coefficient [15]. Although the material properties are temperature independent, to account for the heat loss due to convection

and radiation, a convection coefficient is applied to the sides of every activated layer [15]. An applied constraint is the steady-state heat equation, Equation (2), for which **K** is the heat conduction matrix and **G** is the internal heat generation vector containing heat sources and boundary conditions, explained in Section 3.1. Other constraints of interest regarding the AM process chosen for this demonstration are volume (V(x)) and contact area with the part (A(x)), Equation (3) and Equation (4), respectively. In addition to these constraints, users may consider other design requirements related to the design variables such as uniformity of temperature distribution along the top surface [5] or residual deformation [8,10]. Volume is a commonly used constraint as the support structure is material waste after the part has been removed from the build plate [18,44]. The less material required for the sacrificial material typically results in reduced build cost and build time [45]. Therefore, the optimizer must consider a fraction, ε_v, of the total volume of the design domain, V_{max}. Regarding the contact area, post-processing is also imperative to the design of parts for the build. If support structures are not removed properly, the residue can increase the surface roughness of the part [1,20,46]. For more delicate features such as thin-walled designs, removing excess material from the surface could damage the part [47]. A fraction, ε_A, of the sum of the areas of the part within the design domain on the XY and YZ planes, A_{max}, is considered.

TABLE 1: Properties of various unit cells for AlSi10Mg in comparison to an equivalent solid volume. Advantageous qualities in bold.

Unit Cell	K_{eff} [W/m°C]	Volume [mm³]	$Area_{XY}$ [mm²]	$Area_{YZ}$ [mm²]
Solid	110	8	4	4
SC	12.37	1.82	2.31	2.31
BV	24.39	2.82	0.567	1.30
FC	39.43	3.69	0.846	3.24

Objective 1.2: Constructing expedited evaluation approaches for non-gradient-based optimizers to obtain optimal combinations of lattice structures.

Running a transient model during each iteration for each layer leads to high computational costs, despite the combination of single-layer activation and superlayers [8,43,48]. To combat the high computational cost, a steady-state model can be performed within one step [42,43]. LPBF can be simplified to a system of two parallel plates in which heat moves from one plate (source) to another (sink) [49]. Lattice support structures are employed for the transfer of heat from the source to the sink underneath the cantilever beam. The input boundaries for this approach are the temperature distribution obtained from the transient model to evaluate, from Objective 1.1. This approach is compatible for simple and complex designs [42]; therefore, it will be used in this study for evaluation of the minimization of the heat transfer rate through the base plate. In this model, only heat conduction is considered.

The governing equation for this model is

$$q''=\nabla\cdot(K_{eff}(x)\nabla T(x)), \quad (6)$$

where q" is the internal heat generated by the system, K_{eff} is the effective thermal conductivity, and ∇T is the temperature gradient. To relate the dissipation of heat to a steady-state model, Fourier's heat conduction law,

$$q' = -K_{eff}\, dT/dz, \quad (7)$$

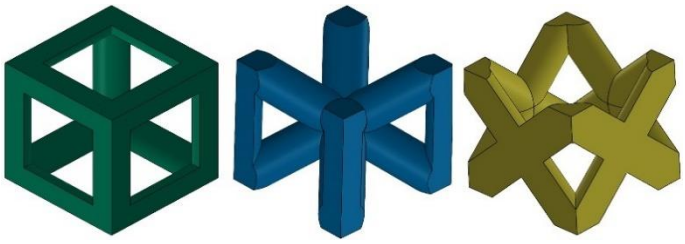

FIGURE 2: Unit cells employed for lattice support structure heat transfer analysis (from left to right): Simple Cubic (SC), Body-Centered Vertical struts (BV), and Face-Centered Cubic (FC)

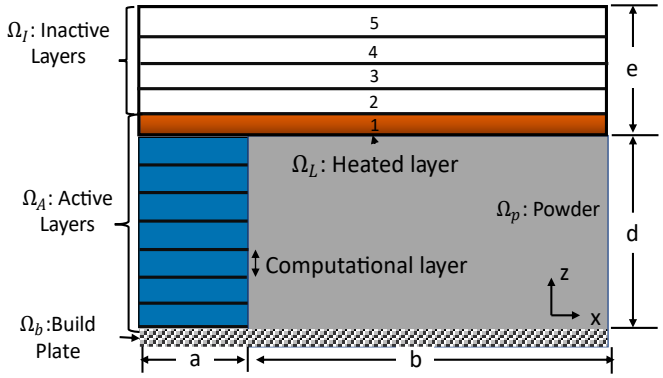

FIGURE 3: 2D schematic of cantilever beam showing the layer-by-layer simulation.

is evaluated as it relates the rate at which heat flows through any surface per unit area, q', with the conductivity, K_{eff}, the temperature difference between the surfaces for the cantilever height of *z*. More specifically, the heat transfer rate, Q_{out}, is calculated by integrating the flux over the area of the element [31]. This problem is numerically solved using the commercial finite element analysis solver, ANSYS.

Given the complexity of the many possible unit cells and configurations within the design domain, a new mesh needs to be generated for each iteration during optimization. An alternative is to use a simpler representative volume with equivalent material properties, namely, the homogenization approximation [50]. The basic idea behind the approach is that the effective (i.e., average) properties of an RVE can be found by mapping the relationship between the entire domain composed of many RVEs to a single RVE (i.e., a unit cell). This requires solving two physics problems, one at the macroscale and one at the microscale, that are coupled by a scaling factor. Two assumptions are made with this approach: (1) the RVE chosen is infinitely small compared to the macroscopic domain, and (2) periodic conditions apply within the macroscopic domain. This procedure has been previously employed in optimization problems to reduce the computational effort for functionally graded [8,25,26,51] and non-graded [27–29] lattices. More information can be found in a review performed by Hassani and Hinton [50].

The SA algorithm begins with a randomized distribution of SC, BV, and FC unit cells that fill the void design domain at the initial state. The initial state is progressively altered iteratively according to the future evaluations of the objective function at a rate defined by the user in the pre-processing stage. The starting temperature, T_0, is defined to initiate the optimization. Further temperature reduction follows the geometric cooling schedule defined as

$$T_{k+1} = \alpha * T'_k, \tag{8}$$

where T'_k is the annealing temperature at the k-th state, T_{k+1} is the temperature at the next state and α is the cooling constant [31]. The probability of acceptance is defined as

$$P_{acc} = exp(-(E_2 - E_1)/T'_k), \tag{9}$$

where E_k and E_{k+1} are the energy states (i.e., objective functions) of the previous state and current state, respectively. To determine the acceptance, the computed probability, P_{acc}, is compared to a randomly generated number between 0 and 1. If P_{acc} is greater than the random number, the inferior design state is accepted; otherwise, it is rejected.

One limitation of the traditional SA algorithm is that it evaluates changes from small changes in the design variables per iteration. With a large design space within the design domain for the lattice support structure, it would be inefficient to optimize by performing only a couple moves (i.e., swap of the unit cell for another randomly chosen unit cell) per iteration given that there are 3^n possible configurations, based on the number of design variables (*n*). Therefore, to encourage a wider search of the design solutions for practical application, an added modification is the number of swaps per iteration that is made to be dependent on the annealing schedule. During the initial stages, a rigorous exploration occurs by setting the number of swaps equivalent to *n*. As T'_k decreases to 1/5th of T_0, the number of swaps decreases to *n*/10. In the final stages of the design, when T'_k is less than 0.5, the number of swaps decreases to one per iteration. These values are selected as they create a steep descent in the objective function. Further study will be needed to investigate other strategies for swapping based on the objective function or the annealing schedule. The stopping criteria of this optimizer are either when T'_k reaches the minimum temperature of 0.1, used for this study, or the maximum number of iterations set by the user is reached.

TABLE 2: Parameters for layer-by-layer application [8]

Process Parameter	Value
Volume heat flux, q" [W/m^3]	2×10^{13}
Convection coefficient for heat loss to environment, h_{side} [W/m^2°C]	400
Convection coefficient for heat loss to build plate, h_{plate} [W/m^2°C]	8,000
Heating time per layer, t_h [s]	6×10^{-4}
Cooling time per layer, t_c [s]	5
Build plate temperature, T_{amb} [°C]	20

Case Study of Cantilever Beam

A case study of a cantilever beam, shown in Figure 1, is employed to validate the optimization process introduced in Objective 1. The dimensions of the cantilever beam for the

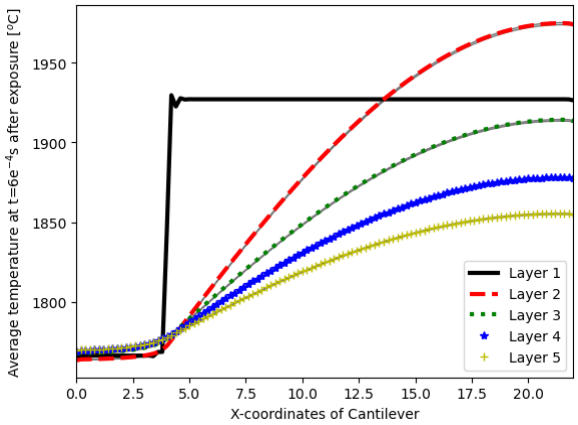

FIGURE 4: Temperature transition of LPBF process: represents temperature at the end of the heating process for all of the computational layers. Extracted from the top of each activated layer.

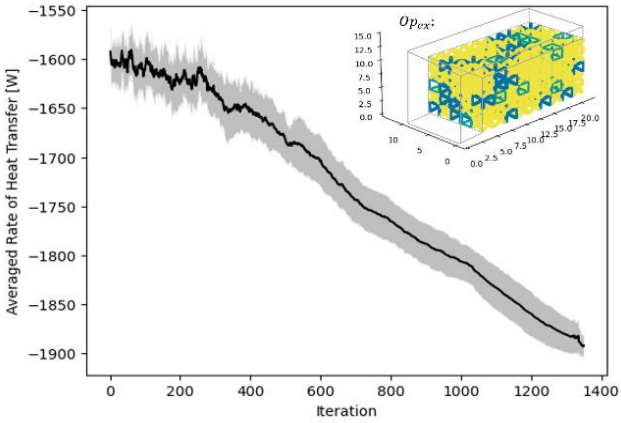

FIGURE 5: Average objective function value for the heat transfer rate with shaded regions showing standard deviation with an example Op_{ex2}, with final values: Objective = -1,900 W, Volume = 615 MM^3, Area = 106 MM^2.

problem defined in Figure 2 are: a = 4 mm, b = 18 mm, c = 10 mm, d = 10 mm, and e = 1 mm. The proposed framework begins with defining the design variables, boundary conditions, and hyperparameters for the optimizer.

By applying the respective process parameters (Table 2) on the surface of the recently activated layer, the averaged y-axis distribution along the x-axis of the cantilever after heating is shown in Figure 5. The five layers of the overhang correspond to the layers labeled in Figure 3. For this study, the temperature distribution across the top of the cantilever for the first layer will be utilized as the applied load for the design domain in the steady-state optimizer evaluation. The last components of the pre-processing steps are performed based on the results from the transient thermal simulation about the design domain. For this demonstration, the design domain is evenly partitioned to allow for a total of 225 geometric design variables. SC, BV, and FC are the uniformly sized unit cells chosen possessing properties outlined in Table 1. The pre-processing stage concludes by defining the main hyperparameters cooling schedule for the annealer as $T_0 = 50$ and $\alpha = 0.5$.

After the inputs are established, the constraints on volume and area are selected as $V_{max} = 750$ and $A_{max} = 140$, respectively. These constraints are chosen to demonstrate how the optimizer may be tuned according to the advantages of each of the unit cells without restricting the design space to a single unit cell configuration. For future applications, practitioners may specify these constraint values based on manufacturing cost and post-processing requirements.

By combining the stage-dependent swapping coupled with the homogenization approximation, the iteration curve appears to have reduced the heat transfer rate of the lattice support structure from its initial state, shown in Figure 6, within 1,400 iterations. A reduced Q_{out} corresponds to a higher dissipation of heat through the system. The optimizer is run 30 times to obtain a statistical average and standard deviations of 1 sigma. Using a desktop computer, Intel Core i7-7700 CPU, each run is approximately 5 hours per simulation resulting in about 12 seconds per iteration. For this size of a simulation, employing the microscopic material distribution with SIMP for optimization would take significantly longer.

The results from the optimization, shown in Table 3, compare the average of 30 optimized designs, Op_{avg}, to the benchmark designs. Starting from a randomized initial state, the optimizer is capable of producing unit cell configurations that have better dissipation than BV Only and SC Only lattice support structures, for both the exact model ($Q_{out,exact}$) and homogenization approximations ($Q_{out,h}$), as shown in Table 4. The dependency on the initial configuration that is typically

TABLE 3: Comparison of the benchmark results to the average of 30 optimized structures for the cantilever beam, Op, with standard deviations shown in parentheses for the optimizer.

	$\|Q_{out}\|$ [W]	**V(x) [mm^3]**	**A(x) [mm^2]**	**SC/BV/FC**	**V(x) < 750 A(x) < 140**
Solid	4,546	1,800	280	0/0/0	No
SC Only	1,196	409	161	225/0/0	No
BV Only	1,607	634	57	0/225/0	Yes
FC Only	2,124	830	120	0/0/225	No
Op_{Avg}	**1,887 (15.)**	**745 (5.5)**	**108 (4.9)**	**18/58/149 (3.2/5.4/5.3)**	**Yes**

found using gradient-based optimizers [16,25] is not found in this approach as there is convergence of the objective function within a relative standard deviation of 0.7%. A limiting factor of this approach is that the predefined library constrains the bounds of achieving better properties than a homogenous structure composed only of the best unit cell property, (e.g., best contact area for BV Only). However, the optimizer leverages the favorable properties of each unit cell to achieve a lattice support structure with an acceptable objective function within the pre-defined constraints. Of the three benchmark lattice structures, BV Only is the only structure that satisfies the predefined constraints, due to its intermediate properties. When compared to BV Only, the heat output of Op_{avg} (absolute value) is 16% higher. Based on the optimized steady-state model, Op_{avg} balances the tradeoffs of the unit cell properties to generate better macroscopic thermal properties for steady-state thermal analysis.

TABLE 4: Comparison of the benchmark results to a randomly selected optimized structure, Op_{ex}, for steady-state heat flow exact and homogenization approximation results and transient exact solution time results

Analysis Model	Simulation	SC Only	BV Only	FC Only	Op_{ex}
Steady-State	$Q_{out,h}$ [W]	1,196	1,607	2,124	1,900
	$Q_{out,exact}$ [W]	1,198	1,605	2,132	1,917
Transient	t_s [s]	3.28	2.18	1.38	1.45

Although a steady-state thermal analysis is employed during the optimization, LPBF is a transient thermal problem; therefore, a transient solution is still needed to assess the time-dependent transfer of heat through the system. A full-scale transient thermal analysis for the application of the first layer is run to further validate the optimized results. The metric chosen to compare the optimized design to the benchmark designs is the time taken for the entire structure to converge to a stable temperature within a 1% difference. All maximum temperatures in the system are reduced to below the melting temperature of AlSi10Mg for both the benchmark and optimal designs; however, the rates at which they cool are just as important in producing stable designs [8]. Table 4 shows that SC Only structure takes the longest time to reach a steady-state temperature at 3.28s. With the highest volume, FC Only dissipates the heat the fastest; whereas Op_{ex} achieves steady-state the second fastest at 1.45s. These results indicate that the framework achieves desirable properties for heat-dissipating lattice support structures while adhering to AM constraints for the transient and steady-state cases.

4. Current Work

4.1. Objective 2: Designing Thermally Conductive Hybrid Lattice Support Structures Constrained by Residual Stress and Deformation for LPBF

Given the multi-functionality of support structures, the inclusion of residual stress mitigation was incorporated into the framework for AlSi10Mg. Coupling the homogenization approximation with stochastic optimization to maximize heat dissipation. A modified simulated annealing is coupled with the homogenization approximation to quickly optimize the distribution of three commonly employed unit cells while adhering to user-defined manufacturing constraints. This model incorporates two sub-models that predict the thermal and mechanical properties of the structure due to the change in unit cell distribution. Two case studies are considered in this demonstration of the framework: a cantilever beam and an aerospace bracket. The additional study of an aerospace bracket considers a higher dimensional problem with multiple design domains to demonstrate the practical application of this framework. For each case, optimal hybrid lattice support structures are consistently obtained with ~14% better heat dissipation and a 25% decrease in distortion for the cantilever beam compared to the uniformly distributed benchmark design with manufacturing constraints satisfied. Preliminary results for the aerospace bracket show a ~5 % increase in heat dissipation and a 29% decrease in distortion while being the only structure to satisfy all constraints compared to the benchmark designs.

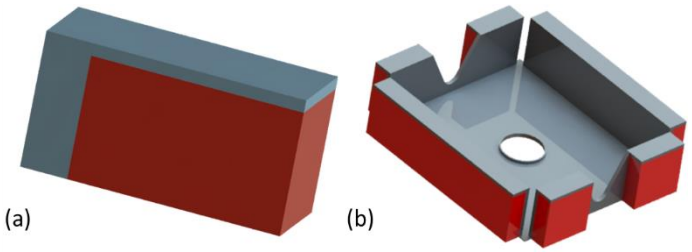

FIGURE 6: 3D representation of the two cases: (a) cantilever beam and (b) bracket

Objective 2.1: Formulating the optimization problem to maximize heat dissipation while considering structural constraints

The cantilever beam, shown in Figure 6a, is a commonly used benchmark for the design of support structures and is

employed here to introduce the modifications to the existing framework established in Section 3.1. Moreover, another case study for a type of aerospace bracket, shown in Figure 6b, is performed [52]. As shown in Figure 6, the volume underneath the overhangs, the volume depicted in red, is denoted as the design domain. Notably, the framework established in this section is generally applicable to the design of other support structures. A flowchart of the modified optimization methodology is illustrated in Figure 7 with the example of the cantilever beam. By optimizing the distribution of individual unit cells, selected from a library, the heat can transfer from the applied heating to the base plate, located at the bottom plane of the cantilever. In addition, the support structure generated within the design domain must also satisfy multiple user-defined manufacturing constraints, which include the structural functionality of support structures.

To integrate the additional mechanical constraint into the optimizer, the problem must be modified. The metric used for the objective statement remains to minimize the heat transfer rate through the base plate, Q_{out}, described in Objective 2.2 and represented as Eq (1). Three additional constraints are considered for the structural functionality of the support structure: governing structural equation, the maximum stress and the maximum total displacement.

$$\text{subject to} \quad \mathbf{EU} = \mathbf{F} \tag{10}$$

$$\sigma_j^{PN}{}_{\max} \leq \sigma_{max} \tag{11}$$

$$U_z \leq U_{max} \tag{12}$$

The equilibrium equation, Eq (10), is comprised of **E**, **U**, and **F**, which are the stiffness matrix, global displacement, and prescribed loading, respectively. Stress constraints are considered by evaluating the maximum normalized von Mises stress within the structure ($\sigma^{vM}{}_{max}$), shown in Eq. (3) using the commonly employed P-norm stress constraint (σ_j^{PN}) [10,53]:

$$\sigma_j^{PN}(x) = \left(\frac{1}{N_j}\sum_{a\in\Omega_j}\left(\sigma_a^{vM}(x)\right)^p\right)^{\frac{1}{p}}. \tag{8}$$

where N_j is the number of stress evaluation points in a set of Ω_j and p is the P-norm factor. The stress level technique for P-norm stress constraint utilized in this work clusters stresses with similar stress levels and compares the average of each *j*

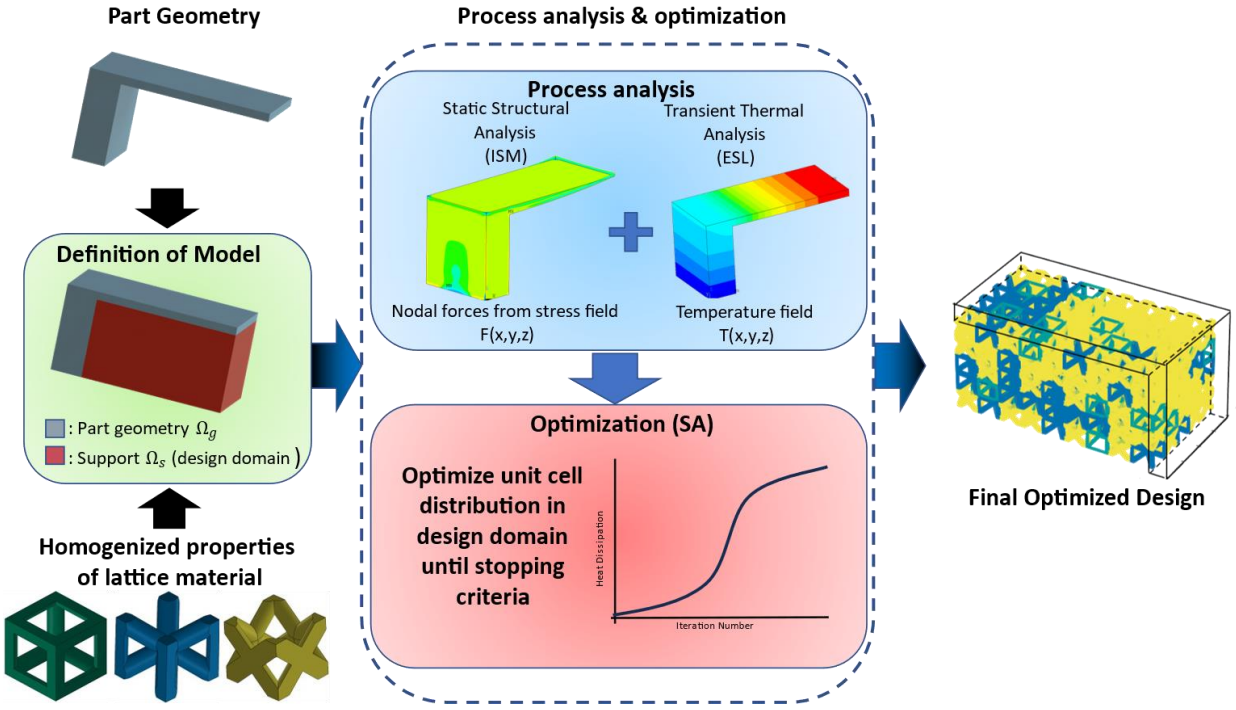

Figure 7: Flowchart summarizing the proposed optimization methodology with part-scale LPBF sub-model simulations for the design of optimized lattice support structure for the cantilever beam.

Table 5: Physical properties of various unit cells for AlSi10Mg in comparison to an equivalent solid volume. Advantageous qualities in bold.

Unit Cell	$K_{eff}\left[\frac{W}{mC}\right]$	E_{eff_z} $[Pa]$	$E_{eff_{Y,X}}$ $[Pa]$	G_{xy} [Pa]	G_{xZ}/G_{yz} [Pa]	$Volume$ $[mm^3]$	$Area_{XY}$ $[mm^2]$	$Area_{YZ}$ $[mm^2]$
Solid	110	7.4E+10	7.4E+10	2.782E+10	2.782E+10	8	4	4
SC	12.37	7.64E+09	7.64E+09	5.419E+08	5.419E+08	**1.82**	2.31	2.31
BV	24.39	9.73E+09	3.69E+09	**4.375E+09**	4.175E+09	2.82	**0.567**	**1.30**
FC	**39.43**	**1.95E+10**	**1.34E+10**	1.598E+08	**6.873E+09**	3.69	0.846	3.24

number of clusters to the maximum stress value [53]. This approach allows for both a local and global analysis of the distribution of stress to prevent stress concentrations. The average stress of each cluster is normalized by the material's yield strength to avoid numerical inaccuracy which may occur due to large changes in stress values.

Knowledge regarding how the part deforms is critical during and after printing. During printing, large upward deformations greater than the layer thickness, L, may damage the re-coater when applying another layer [21–23]. To account for the shrinkage of the powder when melted to a solid layer, a relative powder density, ρ_{shr}, can be applied to calculate the maximum height of deformation [22]. The following equation formulates the maximum z-displacement:

$$U_z = L/\rho_{shr}. \quad (13)$$

After printing, part deformation is imperative to determine whether the part is within tolerance for functionality, particularly on the XY plane where distortion is most prevalent [15,54]. In the traditional manufacturing method of die-casting, a draft angle is a slight slant in the vertical direction of the cast that is used to aid in the removal of parts from a mold [55]. Given that both the cantilever beam and the aerospace bracket can be manufactured using die-casting, the printed design must have a smaller deviation from the original sharp-cornered design than the draft angle required for a traditional die-casted aluminum design. Large draft angles on the XY plane could make manufacturing using LPBF inefficient as opposed to other traditional manufacturing methods. Thus, the maximum deviation in the x and y-direction for the overhang will be the maximum distortion on the XY plane caused by the draft angle needed for parts that are cast. The total maximum deformation will be the magnitude of the maximum displacements in x, y, and z. To obtain the stress and displacement within the system, boundary conditions are applied to a homogenized structure of equivalent dimensions.

$$U_{max} = \sqrt{U_x^2 + U_Y^2 + U_Z^2}. \quad (14)$$

A library composed of three commonly employed unit cells is used for generating the support structure, as defined in Objective 1. Additional material properties regarding mechanical properties are obtained using ANSYS Material Designer. The results of the structure and corresponding material properties are shown in Table 5.

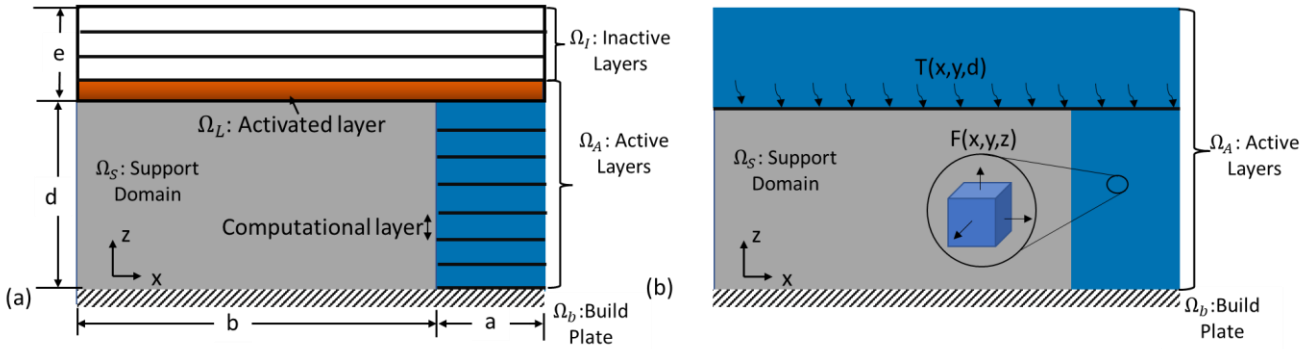

Figure 8: 2D schematic of a cantilever beam showing an example of (a) the layer-by-layer process simulation and (b) input parameters for the model.

Objective 2.2: Predicting both thermal and structural properties of lattice support structures for expedited evaluation using homogenization approximation

In this work, two part-scale models are employed to obtain the inputs for an equivalent static loading: Flash heating and inherent strain methods. The flash heating method, utilized in Objective 1, is employed as the layer-by-layer simulation for the thermal aspect. Temperatures from underneath the area(s) of the overhang are extracted as each subsequent layer is activated with a volumetric heat flux on the top surface.

The inherent strain method (ISM) is a popular technique utilized to predict residual stress for single-layer, welded metal parts. More recently, it has also been applied to metal AM printing techniques and has shown to be a promising approach for mechanical property prediction due to its speed and accuracy for part-scale models, compared to a full thermomechanical analysis [10,21–23,56]. The input values of this method are extracted from the temperature history of a small-scale thermal analysis, for which temperature-dependent properties are considered. A modified ISM method was proposed by Liang *et al.* [54] and will be employed with properties found in [16]. For this approach, a quasi-static mechanical analysis is performed by applying a layer-by-layer activation of an external load with boundary constraints on each activated element layer, i. The governing equation for ISM analysis is:

$$\begin{cases} \nabla \cdot \sigma_i = 0 & (15) \\ \sigma_i = E\varepsilon_e^i & (16) \\ \varepsilon_{tot}^i = \varepsilon_e^i + \varepsilon_p^i + \varepsilon_{in}^i, & (17) \end{cases}$$

where σ_i denotes the stress field for the i-th activated layer and E is the constitutive elastic tensor. The elastic, plastic, inherent, and total strain field for the i-th layer are denoted as $\varepsilon_e^i, \varepsilon_{in}^i$, and ε_p^i, respectively. The sequential analysis takes the solution from the previous step as an input boundary condition for the current step. After the quasi-static simulation is completed, the force values of the part are extracted to be input for the static equivalent loading.

One major underlying assumption of this model is that the average inherent strain values, applied as the coefficient of thermal expansion within the ANSYS model, are constant [54]. Therefore, applications of ISM on an overhang void of support structure would result in inaccurate results. To address this challenge while still adhering to applied assumptions, a uniformly distributed lattice support structure of the weakest unit cell is placed underneath the overhang. The lattice support structure is assumed to have the same inherent strain vectors as the bulk material [8]. After simulation, the force values of the part are extracted to be input for the static equivalent loading [21].

Although ISM is notably faster than a full-scale thermomechanical model, large complex structures may still take hours to evaluate [16]. This deems the approach as impractical for generalized use within the highly iterative optimization process. Therefore, the sub-model will be evaluated in one step by inputting the nodal force from the part into the mesh as an input force. The following governing equation is solved using the FEM solver, ANSYS:

$$\nabla \cdot \sigma + F = 0. \quad (18)$$

In Eq (18), σ denotes the stress field and F is the applied force load vector. The force and stress at each node are extracted from the part based on the displacement solution. The von Mises equivalent stress is utilized for this model to consider the yield criterion. However, users may also choose to solve Hill's yield criterion [8,57]. To reduce computational time, The forces from the ISM are extracted from only the part and applied as a load to the optimization model domain. For each iteration within optimization, the p-norm stress and the maximum total displacement are evaluated. If the model exceeds the structural, volume, or area constraints, the design is rejected.

Case Study of Cantilever Beam

The cantilever beam is a commonly employed benchmark design for the study of support structures, as shown in Figure 6a. The pre-optimization steps, outlined in Objective 1, are first performed to determine the input values for each sub-model's equivalent static analyses. The hyperparameters chosen are $T_0 = 50$ and $\alpha = 0.5$. Beginning with the thermal analysis, a part-scale layer-by-layer simulation is performed for the same cantilever beam of dimensions as described in Objective 1. After each layer is activated utilizing the new process parameters (Table 6), the temperature underneath the

overhang is extracted from the model after heating, averaged across the length of the overhang, and plotted in Figure 9. For the equivalent static load, the temperature from layer 1 activation is taken as input as it is the worst temperature.

The layer-by-layer structural analysis is also performed with inherent strain vector inputs from Table 6. After all activations are performed, the forces of only the cantilever beam are extracted as input for the model. It should be noted that in this approach, the underlying assumption is that the forces are support design independent as the design space is filled with only SC structures. However, the trend of the distribution of force is captured to show the generalized reaction of the cantilever's overhang when the structural analysis is performed.

TABLE 6: Parameters for layer-by-layer application

Process Parameter	Value
Volume heat flux, q $[W/m^3]$	1.96×10^{13}
Convection Coefficient for heat loss to environment, h_{side} $[W/m^2°C]$	100
Convection Coefficient for heat loss to build plate, h_{plate} $[W/m^2°C]$	8000
Heating time per layer, t_h[s]	4×10^{-4}
Cooling time per layer, t_c [s]	5
Build plate temperature, T_{amb} [°C]	20
Inherent strain vector in x, y, z	-0.016,-0.016, 0.014

Next, initialization of the structure is performed to fill the design domain with a randomized configuration. The objective function is then evaluated and the optimization procedure begins. For this case, the stage-dependent number of swaps begins with a rigorous design exploration of swaps with 225, equal to the number of design variables, *n*. During the intermediate phase, the number of swaps decreases to *n*/10 whereas the tuning stage ends with one swap per iteration. When the stopping criterion has been reached, the results are compared to the steady-state simulations. The results of this simple case demonstrate the promise of this framework.

With the input from the two sub-models obtained and the optimization, the procedure begins with the randomized material distribution. The amount of heat dissipation from the cantilever to the build plate is measured as the minimization of heat transfer rate out of the system, Q_{out} through conduction only. According to the National Aeronautics and Space Association (NASA), the safety factor for aerospace components is 1.5 [58]; therefore, the maximum stress is set at 0.66. To calculate the P-norm, p = 15. Given the L = 30μm and ρ_{shr}= 1 the absolute maximum z-displacement, U_z, is set to 30 μm. The maximum deviation of 1° [55] (i.e. U_x = U_y = 8μm) is chosen for the top overhang, resulting in U_{max} = 32 μm. The constraints on volume and interfacial area are selected as V_{max} = 750 and A_{max} = 140, respectively.

Table 7 shows the results from the optimization which compares the average of 30 optimized designs, Op_{avg2}, to the uniformly distributed benchmark designs. The results indicate that the optimizer satisfies all the user-defined constraints and achieves an average of 14% better dissipation and a 25% reduced deformation than BV Only, the intermediate unit cell. These results are expected as FC is the most favorable unit cell to achieve the highest heat dissipation and stiffest structure. Although the cantilever beam is a benchmark structure, it does not exploit the capabilities of LPBF for larger structures with multiple support domains as shown next with the aerospace bracket.

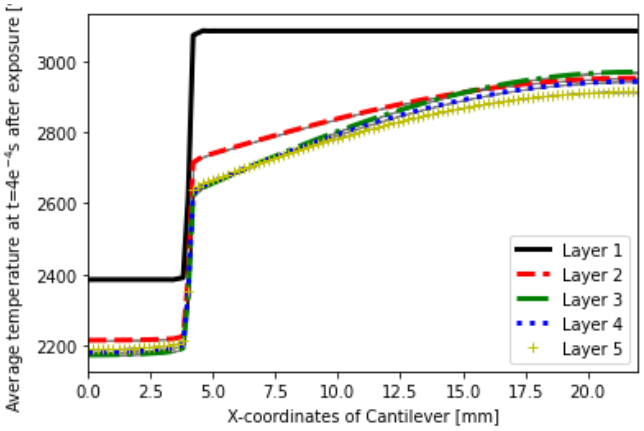

FIGURE 9: Temperature transition of LPBF process: represents temperature at the end of the heating process for the computational layers extracted from underneath overhang of cantilever beam.

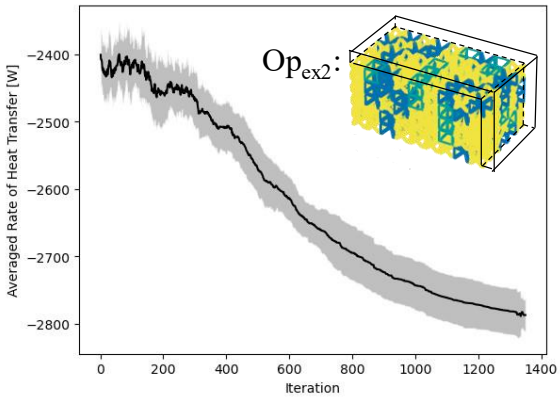

FIGURE 10: Average objective function value for the heat transfer rate with shaded regions showing standard deviation with an example Op_{ex2}, with final values: Objective = -2,815 W, Volume = 735 mm^3, Area = 108 mm^2, p-Norm = 0.366, U_{sum} = 24.2 mm

Table 7: Comparison of the benchmark results to the average of 30 optimized structures for the cantilever beam, $Op_{avg,2}$, with standard deviations shown in parentheses for the optimizer.

	$\|Q_{out}\|$	V(x)	A(x)	P-norm Stress	Max(U_{sum}) [µm]	SC/BV/FC	V(x)<750 A(x)<140 P-norm < 0.66 Max(U_{sum}) < 32
Solid	7,128	1,800	280	0.293	8.06	--	No
SC	1,743	409	161	0.359	31.7	225/0/0	No
BV	2,405	634	57	0.365	30.8	0/225/0	Yes
FC	3,235	830	120	0.352	15.6	0/0/225	No
$Op_{avg,2}$	**2,773 (47.1)**	**722 (11.7)**	**107 (6.82)**	**0.360 (0.00614)**	**24.0 (1.34)**	**27/63/133 (5.3/8.0/9.4)**	**Yes**

Case Study of Aerospace Bracket

The aerospace bracket is chosen for demonstration of this framework as it provides a practical case in which the dimensionality of the problem is high and there are multiple overhangs to consider. Following the outlined framework used by the cantilever beam, pre-processing is performed to obtain the optimizer inputs. The hyperparameters chosen are T_0 = 50 and α = 0.5. Next, initialization of the structure is performed to fill the design domain with a randomized configuration. For this case, the stage-dependent number of swaps begins with a rigorous design exploration of swaps with 1,776, also equal to the number of design variables, *n*. During the intermediate phase, the number of swaps decreases to *n*/100. As opposed to the single swapping in the cantilever beam case, the swaps are set to *n*/200. This modification was chosen because single swaps in such a large domain would not have as significant of an impact on the objective function as it would in a small domain. Further study will be needed for a more precise evaluation of the impact factor of the number of swaps on the model's ability to reach an optimal state. When the stopping criteria has been reached, the results are compiled and compared to the benchmark designs of uniform lattices. The results of this more complex case demonstrate the practicality of this framework.

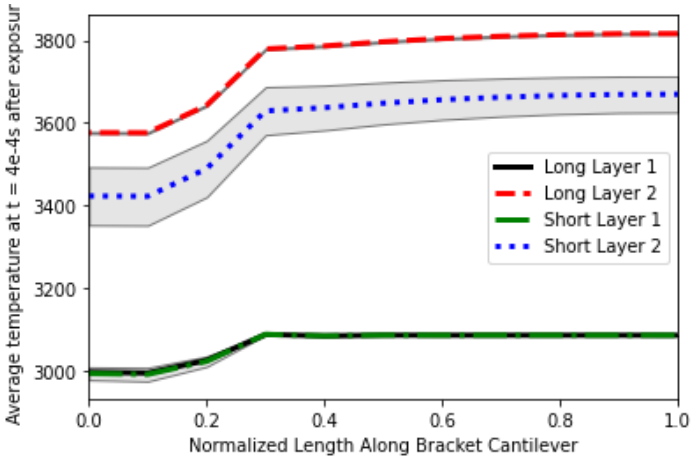

FIGURE 11: Temperature transition of LPBF process: represents temperature at the end of the heating process for the computational layers extracted from underneath overhang of aerospace bracket.

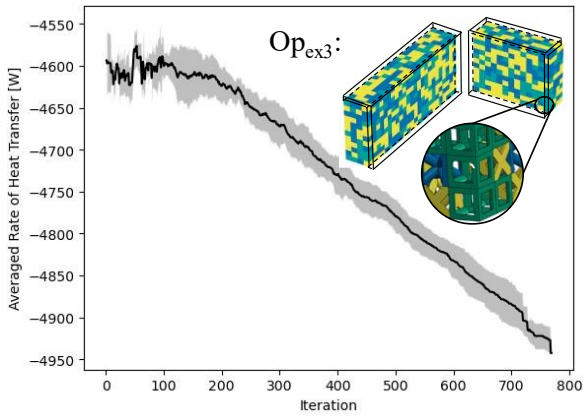

FIGURE 12: Average objective function value for the heat transfer rate with shaded regions showing standard deviation with an example $Op_{avg,3}$, with final values: Objective = -4,860 W, Volume = 5,264 mm^3, Area = 1,201 mm^2, Displacement = 74 µm and P-norm = 0.646

Table 8: Comparison of the benchmark results to the average of 5 optimized structures for the aerospace bracket, $Op_{avg,3}$, with standard deviations shown in parentheses for the optimizer.

	$\|Q_{out}\|$	V(x)	A(x)	P-norm Stress	Max(U_{sum}) [μm]	SC/BV/FC	V(x) < 5,900 A(x) < 1,360 P-norm < 0.66 Max(U_{sum})< 76
Solid	12,479	14,208	2,368	0.609	14	--	No
SC	3,524	3,232	1,367	0.648	96.0	1,776/0/0	No
BV	4,624	5,008	661	0.648	97.5	0/1,776/0	No
FC	6,004	6,553	1,568	0.637	74.7	0/0/1,776	No
$Op_{avg,3}$	**4,902 (29.4)**	**5,315 (36.2)**	**1,222 (13.7)**	**0.643 (0.0037)**	**72.8 (2.3)**	**388/589/799 (16/20/30)**	**Yes**

The procedure utilized for the pre-processing of the cantilever beam sub-model inputs is followed for the aerospace bracket. Given the two planes of symmetry of the bracket, a quarter of the bracket is modeled to reduce computational cost. The part-scale layer-by-layer flash heating is performed for the two overhangs (i.e., long and short) with an average element size of 1 mm^3. The long overhang has dimensions: a = 2 mm, b = 8 mm, c_{long} = 48 mm, d = 24 mm, e = 2 mm. The short overhang has the same a, b, d, and e dimensions but the length of the overhang, c_{short}, is set to 26 mm. The temperature underneath the overhang is also extracted from the model after heating and plotted in Figure 11. The temperature distribution trend for both the long and short overhangs is similar but the short cantilever has reduced temperature due to the amount of accumulated heat and dissipation through bulk material on one side of the structure. As with the cantilever beam, the default support structure utilized for the ISM layer activation is a uniform distribution of SC with homogenized properties. The forces of both overhang structures are extracted as input for the model.

Given the change in the design space geometry and design variables, the constraints must change accordingly. The maximum stress is still set to 0.66 with p = 8. The maximum deviation of 1° for Ux and Uy (i.e. 34 μm). The relative density ρ_{sh} is set to 0.5 [22], yielding U_{max} = 76 μm. The volume constraint is set to V_{max} = 5,900 mm^3 and the interfacial area is selected to be A_{max} = 1,360 mm^2. Utilizing the inputs from the sub-models, the initialization is performed and optimization begins. Each run is approximately 10 hours per simulation.

The iteration history of 5 averaged optimized structures is plotted in Figure 12 and compared in Table 8 with the benchmark designs. When comparing the uniformly distributed structures to the averaged optimized structure, Op_{avg3} is the only structure that satisfies all the constraints. Compared to BV Only, Op_{avg} has a 5% increase in heat dissipation while also achieving a 29% decrease in deformation. Like the cantilever beam, the FC unit cells are favored to achieve a higher dissipation of heat. The continuously decreasing slope in Figure 12 indicates that by tuning the model to increase the number of iterations, even more optimal results could be achieved. The results from this work show the promise of the SA optimizer for problems with thousands of design variables and multiple support structures.

Future work of these case studies will include the validation of the optimized structures using the part scale models.

4.2. Objective 3: Extending Lattice Support Structure Design to Curved Interfaces

Preliminary work in Sections 3 and 4.1, demonstrates the capabilities of the framework for generating lattice support structures for both single and double support domains made of commonly printed AlSi10Mg. In practice, more complex structures are manufactured by LPBF using vastly different materials that would benefit from lattice support structures. Therefore, the last elements of this work are to incorporate curved structures into the model using a new material.

The proposed framework must be applied within industrial settings for which the accuracy of the predicted results for complex structures is critical. In this work, a complex structure is defined as a convex or concave surface (e.g. line or curve) that satisfies the overhang angle requirement of 45° along the build direction. Thus, a modified procedure to fit lattice support structures to non-horizontal overhangs comprised of nickel-based alloy Haynes 282, will be proposed. To this end, the inherent strain input vectors will be recalculated with the intention of utilizing an existing small-scale thermo-mechanical model and experimental data. Modifications will also be needed to generate lattice support structures for the new support domains. Three potential solutions will be investigated to determine the most efficient approach before optimization is

performed. It is intended to incorporate empirical information into the structural analysis to allow for accurate predictions of the residual deformation. If possible, the thermomechanical simulation will be run to obtain an initial guess pertaining to the inherent strain vectors then a regression analysis will be performed to fit the properties of the computational model to the experimental results. After optimization is run, the results will be compared to the traditional support structure.

Objective 3.1: Generating results for inherent strain inputs for arbitrary materials

LPBF can manufacture a variety of metals with different material properties. As new materials continue to be discovered, support design generators must be adaptable. To demonstrate the adaptability of this framework will incorporate a methodology on utilizing Ni-based superalloy Haynes 282. Compared to AlSi10Mg, Hanyes 282 is a relatively new material to be manufactured using LPBF. It has high strength at elevated temperatures and high resistance to corrosion and oxidation [59], making it ideal for applications such as industrial gas turbines [60]. Novelty and practicality make this material fitting to demonstrate the applications of the framework for multiple materials.

Optimizing the support structure for a new material will require new inherent strain vectors for the quasi-static structural model to obtain the input forces. These values can be obtained using purely computational [54] or empirically informed computational [61,62] methods. For the purely computational approach, a thermomechanical model may be utilized to simulate a two-layer print [54]. The approach to applying ISM is based on the work performed by *Liang et. al.*[54], for which the inherent strain is a combination of the plastic, elastic, and inherent strain at the bottom of the layer after deposition, as seen in Eq (15-17). The average total strain in x, y, and z is then normalized by the corresponding dimensions of the layer to be applied in the ANSYS static structural analysis.

It is intended that a hybrid model, utilizing empirical results, is integrated into the optimization procedure to obtain the inherent strain vectors. The empirical results could be obtained by printing and cutting cantilever beam coupons to obtain the change in deformation along the length [61]. The inherent strain vectors will be calculated by fitting the deformation results from the quasi-static mechanical model to the empirical results. Figure 13 demonstrates a brief overview of the computational procedure to predict the deformation for AlSi10Mg.

In the case that the thermomechanical model is performed and the empirical results are obtained, the thermomechanical model results will be used as the initial guess for the curve-fitting regression model.

Contingency Plan

1. If a thermomechanical model cannot be run, the inherent strain vectors will be obtained from literature using material of similar properties to Haynes 282, such as Inconel 718 [59].
2. If experimental results cannot be obtained, the thermomechanical model will be utilized as ground truth.

Objective 3.2: Incorporating complex structures into lattice support structure design framework

A major advantage of LPBF is its ability to manufacture complex structures; therefore, support for these structures is critical to the process and the proposed framework. The complexity considered in this work will be defined as asymmetric, curved parts. For this, a modified approach to support structure design must be proposed. Current work utilizes three unit cells of uniform size; however, this is not sufficient for parts with curves or angles as full unit cells would have a small contact area with the part resulting in the inefficient transfer of heat. Therefore, several potential solutions, shown in Figure 14, will be investigated: size change, additional unit cells, and forced flat domain. Changing the size of the unit cell allows for reduced open spaces in which the larger cells cannot fill, without the added complexity of fractional cells [39]. A

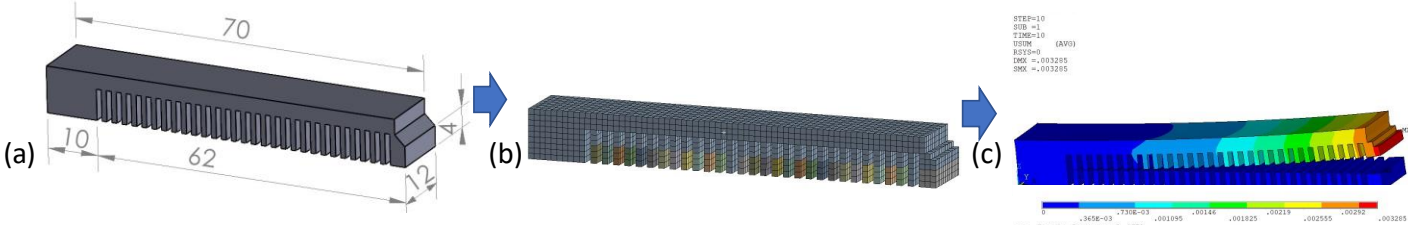

Figure 13: Example of simulation procedure to obtain deformation results on (a) cantilever coupon that is (b) voxelized into 1 mm^3 elements then, using input inherent strain vectors for AlSi10Mg, Table 6, the displacement along the cantilever is predicted.

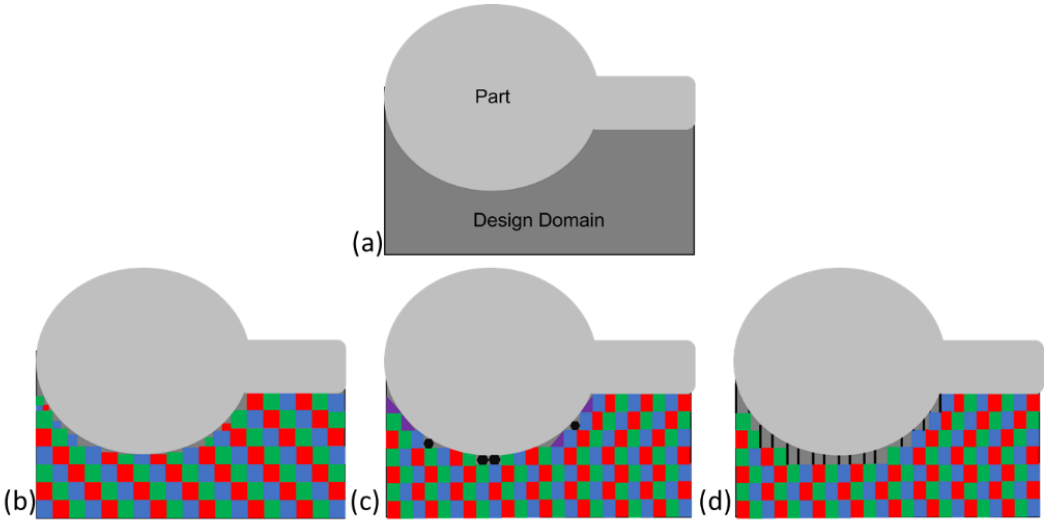

Figure 13: 2D schematic of potential solutions for (a) an asymmetric, curved structure with design domain using (b) size varying lattices, (c) additional unit cells (d) forced flat domains.

potential challenge to be overcome would be the range of sizes. These could be addressed by considering additional unit cells for the existing library. For example, octahedron and rhombic dodecahedron unit cells have been employed for design of support structures to hold up parts while considering support removal [63]. The previous approaches may still have problems when considering the direct connection to the curved surface. Therefore, the last solution that will be explored is to use a pin or solid support for direct connection to the part to form flat surfaces for unit cell connection [6]. Either in combination with the size changing and/or additional unit cells, the forced flat domain is the most promising approach.

Objective 3.3: Validating the framework through experimental components.

Lattice support structures will be generated for many complex components. Deformation results from the simulation are intended to be printed and compared with physical models.

Contingency Plan

In the case that experimental results cannot be obtained, models from existing literature will be utilized for a comparative study or full-scale models will be performed on existing designs.

Expected Contributions

Completion of this objective would result in a completed framework that will be an alternative approach to design support structure for AM of components with overhang features. The expected contribution of this framework contributes to the field of design, lattice structure generation, and design for additive manufacturing by advancing the knowledge of:

1. Factors that contribute to design for AM: constraint definitions to consider material waste, post-processing, dissipation of heat and structural integrity.
2. Computational modeling of transient loading to an equivalent static loading: Incorporating two sub-models to reduce iterative evaluation time.
3. Advancing the application of non-gradient-based optimizers within AM: creating lattice structures with tailorable properties that can be evaluated using homogenization approximation with stage-dependent actions to reduce the time for design exploration
4. Coupling experimental results within optimization: Calibration of inherent strain vectors which are inputted into the optimization evaluation for accuracy of the model.

4.3.Timeline

The anticipated timeline for this proposed objective is outlined in Figure 15.

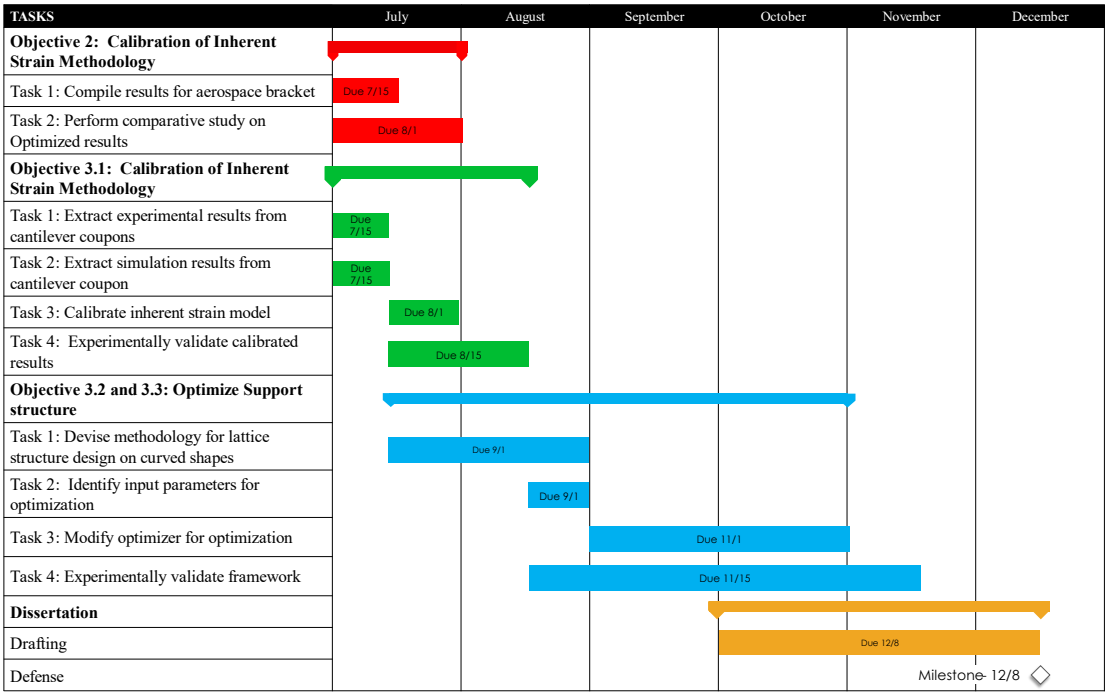

Figure 15: Anticipated timeline for proposed work.

5. Intellectual Merit

Hybrid lattices are a promising type of support structure that possesses tunable properties of individual unit cells at a microscopic and mesoscopic scale. They enable users to consider design constraints for the AM procedure such as the limitation on material waste, removal of support, and deformations that can accrue. However, their full potential has yet to be exploited within LPBF due to limitations in current design approaches. By restricting design variables to a continuous domain, current gradient-based optimizer approaches are limited to one type of unit cell, albeit periodic or with changing densities. This is attributed to the need for differentiable design variables. However, non-gradient-based optimizers find solutions with a higher exploration of various design configurations because there are no restrictions to the types of design variables. Yet, non-gradient-based optimizers have not been applied to the generation of support structures to consider major support structure functionality to reduce heat dissipation and anchor the part to the build plate. Therefore, this proposal seeks to address the gaps described by proposing a new framework for the design of lattice support structures.

By utilizing pre-defined, self-supporting unit cells, lattice structures will be generated with predictive mechanical properties. Constraints employed within this framework will also provide insight for designers to consider important costs when designing for AM. For example, the framework aims to constrain the total volume of material utilized and the amount of area interfacing between the support structure and the part. Volume is directly associated with the cost of material and the cost of machine usage; therefore, constraining the volume with constraining the cost of manufacturing the part. Post-processing is critical when considering cost as support structure may require extensive amounts of finishing to remove excess material that causes surface roughness. By constraining these two features of the optimizer, the framework will improve the economic efficiency of AM technology and make it more friendly to our environment and society. Further, it will contribute to the sustainable development of U.S. manufacturing, and manufacturing companies in the Greater Pittsburgh Region will ultimately benefit from its outcomes.

Dissertation Chapter Outline

1. Introduction and Motivation
2. Coupling Simulated Annealing and Homogenization to Design Thermally Conductive Hybrid Lattice Support Structures for LPBF
3. A Modified Simulated Annealing-Based Optimization to Design Heat Dissipating Hybrid Lattice Support Structures

4. Empirically Informed Optimization of Lattice Support Structures for Complex Parts for LPBF
5. Conclusions and Future Work

6. Acknowledgements

Lisha White is funded by the GEM Consortium.

7. References

[1] Vafadar, A., Guzzomi, F., Rassau, A., and Hayward, K., 2021, "Advances in Metal Additive Manufacturing: A Review of Common Processes, Industrial Applications, and Current Challenges," Applied Sciences, **11**(3), p. 1213.

[2] Grasso, M., and Colosimo, B. M., 2017, "Process Defects and in Situ Monitoring Methods in Metal Powder Bed Fusion: A Review," Meas. Sci. Technol., **28**(4), p. 044005.

[3] Liang, H., Raymont, D., Chunze, Y., Hussein, A., and Young, P., eds., 2011, *Design and Additive Manufacturing of Cellular Lattice Structures*, CRC Press.

[4] Mirzendehdel, A. M., and Suresh, K., 2016, "Support Structure Constrained Topology Optimization for Additive Manufacturing," Computer-Aided Design, **81**, pp. 1–13.

[5] Craeghs, T., Clijsters, S., Kruth, Jean.-P., Bechmann, F., and Ebert, Marie.-C., 2012, "Detection of Process Failures in Layerwise Laser Melting with Optical Process Monitoring," Physics Procedia, **39**, pp. 753–759.

[6] Huang, R., Dai, N., Cheng, X., and Wang, L., 2020, "Topology Optimization of Lattice Support Structures for Heat Conduction in Selective Laser Melting," Int J Adv Manuf Technol, **109**(7–8), pp. 1841–1851.

[7] Wang, D., Wei, X., Liu, J., Xiao, Y., Yang, Y., Liu, L., Tan, C., Yang, X., and Han, C., 2022, "Lightweight Design of an AlSi10Mg Aviation Control Stick Additively Manufactured by Laser Powder Bed Fusion," Rapid Prototyping Journal, **28**(10), pp. 1869–1881.

[8] Lee, K.-Hyun., and Yun, G. J., 2022, "Design Optimization of Thermally Conductive Support Structure for Laser Powder-Bed Fusion Process with Part-Scale Thermal History," Additive Manufacturing, **51**, p. 102627.

[9] Hussein, A., Hao, L., Yan, C., Everson, R., and Young, P., 2013, "Advanced Lattice Support Structures for Metal Additive Manufacturing," Journal of Materials Processing Technology, **213**(7), pp. 1019–1026.

[10] Cheng, L., Liang, X., Bai, J., Chen, Q., Lemon, J., and To, A., 2019, "On Utilizing Topology Optimization to Design Support Structure to Prevent Residual Stress Induced Build Failure in Laser Powder Bed Metal Additive Manufacturing," Additive Manufacturing, **27**, pp. 290–304.

[11] Vaissier, B., Pernot, J.-P., Chougrani, L., and Véron, P., 2019, "Genetic-Algorithm Based Framework for Lattice Support Structure Optimization in Additive Manufacturing," Computer-Aided Design, **110**, pp. 11–23.

[12] Feng, R., Liu, F., Xu, W., Ma, M., and Liu, Y., 2016, "Topology Optimization Method of Lattice Structures Based on a Genetic Algorithm," Int J Steel Struct, **16**(3), pp. 743–753.

[13] Nazir, A., Abate, K. M., Kumar, A., and Jeng, J.-Y., 2019, "A State-of-the-Art Review on Types, Design, Optimization, and Additive Manufacturing of Cellular Structures," Int J Adv Manuf Technol, **104**(9), pp. 3489–3510.

[14] Gouge, M., Denlinger, E., Irwin, J., Li, C., and Michaleris, P., 2019, "Experimental Validation of Thermo-Mechanical Part-Scale Modeling for Laser Powder Bed Fusion Processes," Additive Manufacturing, **29**, p. 100771.

[15] Li, C., Liu, J. F., Fang, X. Y., and Guo, Y. B., 2017, "Efficient Predictive Model of Part Distortion and Residual Stress in Selective Laser Melting," Additive Manufacturing, **17**, pp. 157–168.

[16] Liang, X., White, L., Cagan, J., Rollett, A. D., and Zhang, Y. J., 2023, "Unit-Based Design of Cross-Flow Heat Exchangers for LPBF Additive Manufacturing," Journal of Mechanical Design, **145**(1), p. 012002.

[17] Ameen, W., Mohammed, M. K., Al-Ahmari, A., Ahmed, N., and Mian, S. H., 2020, "Investigation of Support Structure Parameters and Their Affects during Additive Manufacturing of Ti6Al4V Alloy via Electron Beam

Melting," Proceedings of the Institution of Mechanical Engineers, Part L: Journal of Materials: Design and Applications, p. 1464420720981668.

[18] Bartsch, K., Ohrenberg, J., and Emmelmann, C., 2020, "Benchmark Parts for the Evaluation of Optimized Support Structures in Laser Powder Bed Fusion of Metals," Procedia CIRP, **94**, pp. 254–259.

[19] Chen, H., Gu, D., Xiong, J., and Xia, M., 2017, "Improving Additive Manufacturing Processability of Hard-to-Process Overhanging Structure by Selective Laser Melting," Journal of Materials Processing Technology, **250**, pp. 99–108.

[20] Triantaphyllou, A., Giusca, C. L., Macaulay, G. D., Roerig, F., Hoebel, M., Leach, R. K., Tomita, B., and Milne, K. A., 2015, "Surface Texture Measurement for Additive Manufacturing," Surf. Topogr.: Metrol. Prop., **3**(2), p. 024002.

[21] Zhang, Z.-D., Ibhadode, O., Ali, U., Dibia, C. F., Rahnama, P., Bonakdar, A., and Toyserkani, E., 2020, "Topology Optimization Parallel-Computing Framework Based on the Inherent Strain Method for Support Structure Design in Laser Powder-Bed Fusion Additive Manufacturing," Int J Mech Mater Des, **16**(4), pp. 897–923.

[22] Misiun, G., van de Ven, E., Langelaar, M., Geijselaers, H., van Keulen, F., van den Boogaard, T., and Ayas, C., 2021, "Topology Optimization for Additive Manufacturing with Distortion Constraints," Computer Methods in Applied Mechanics and Engineering, **386**, p. 114095.

[23] Pellens, J., Lombaert, G., Michiels, M., Craeghs, T., and Schevenels, M., 2020, "Topology Optimization of Support Structure Layout in Metal-Based Additive Manufacturing Accounting for Thermal Deformations," Struct Multidisc Optim, **61**(6), pp. 2291–2303.

[24] Sigmund, O., and Maute, K., 2013, "Topology Optimization Approaches," Struct Multidisc Optim, **48**(6), pp. 1031–1055.

[25] Cheng, L., Liu, J., Liang, X., and To, A. C., 2018, "Coupling Lattice Structure Topology Optimization with Design-Dependent Feature Evolution for Additive Manufactured Heat Conduction Design," Computer Methods in Applied Mechanics and Engineering, **332**, pp. 408–439.

[26] Cheng, L., Liu, J., and To, A. C., 2018, "Concurrent Lattice Infill with Feature Evolution Optimization for Additive Manufactured Heat Conduction Design," Struct Multidisc Optim, **58**(2), pp. 511–535.

[27] Dos Reis, F., and Karathanasopoulos, N., 2022, "Inverse Metamaterial Design Combining Genetic Algorithms with Asymptotic Homogenization Schemes," International Journal of Solids and Structures, **250**, p. 111702.

[28] Nguyen, J., Park, S., and Rosen, D., 2013, "Heuristic Optimization Method for Cellular Structure Design of Light Weight Components," Int. J. Precis. Eng. Manuf., **14**(6), pp. 1071–1078.

[29] Salonitis, K., Chantzis, D., and Kappatos, V., 2017, "A Hybrid Finite Element Analysis and Evolutionary Computation Method for the Design of Lightweight Lattice Components with Optimized Strut Diameter," Int J Adv Manuf Technol, **90**(9), pp. 2689–2701.

[30] Liang, X., To, A. C., Du, J., and Zhang, Y. J., 2021, "Topology Optimization of Phononic-like Structures Using Experimental Material Interpolation Model for Additive Manufactured Lattice Infills," Computer Methods in Applied Mechanics and Engineering, **377**, p. 113717.

[31] Porter, J. M., Larsen, M. E., and Howell, J. R., 2009, "Discrete Optimization of Radiant Heaters with Simulated Annealing," American Society of Mechanical Engineers Digital Collection, pp. 903–908.

[32] Eberhard, P., Schiehlen, W., and Bestle, D., 1999, "Some Advantages of Stochastic Methods in Multicriteria Optimization of Multibody Systems," Archive of Applied Mechanics, **69**(8), pp. 543–554.

[33] Gosselin, L., Tye-Gingras, M., and Mathieu-Potvin, F., 2009, "Review of Utilization of Genetic Algorithms in Heat Transfer Problems," International Journal of Heat and Mass Transfer, **52**(9), pp. 2169–2188.

[34] Pandey, H. M., Chaudhary, A., and Mehrotra, D., 2014, "A Comparative Review of Approaches to Prevent Premature Convergence in GA," Applied Soft Computing, **24**, pp. 1047–1077.

[35] Campbell, M. I., Amon, C. H., and Cagan, J., 1997, "Optimal Three-Dimensional Placement of Heat Generating Electronic Components," Journal of Electronic Packaging, **119**(2), pp. 106–113.

[36] Liu, M., Shi, Y., Yan, J., and Yan, Y., 2017, "Lattice Boltzmann Simulation of Flow and Heat Transfer in Random Porous Media Constructed by Simulated Annealing Algorithm," Applied Thermal Engineering, **115**, pp. 1348–1356.

[37] Kirkpatrick, S., Gelatt, C. D., and Vecchi, M. P., 1983, "Optimization by Simulated Annealing," Science, **220**(4598), pp. 671–680.

[38] Lee, G., Joo, Y., and Kim, S. J., 2021, "On the Objective Function for Topology Optimization of Heat Sinks," IEEE Transactions on Components, Packaging and Manufacturing Technology, **11**(11), pp. 1776–1782.

[39] Boos, E., Ihlenfeldt, S., Milaev, N., Bruns, M., and Elsner, B. A. M., 2023, "Simulation-Based Support Generation for Laser Powder Bed Fusion Processes," 3D Printing and Additive Manufacturing, p. ahead of print.

[40] Downing, D., Leary, M., McMillan, M., Alghamdi, A., and Brandt, M., 2020, "Heat Transfer in Lattice Structures during Metal Additive Manufacturing: Numerical Exploration of Temperature Field Evolution," RPJ, **26**(5), pp. 911–928.

[41] Echeta, I., Feng, X., Dutton, B., Leach, R., and Piano, S., 2020, "Review of Defects in Lattice Structures Manufactured by Powder Bed Fusion," Int J Adv Manuf Technol, **106**(5–6), pp. 2649–2668.

[42] Subedi, S. C., Shahba, A., Thevamaran, M., Thoma, D. J., and Suresh, K., 2022, "Towards the Optimal Design of Support Structures for Laser Powder Bed Fusion-Based Metal Additive Manufacturing via Thermal Equivalent Static Loads," Additive Manufacturing, **57**, p. 102956.

[43] Bartsch, K., Herzog, D., Emmelmann, C., and Lange, F., 2019, "A Novel Approach to Support Structures Optimized for Heat Dissipation in SLM by Combining Process Simulation with Topology Optimization," The NAFEMS World Congress Quebec City, Quebec, QC, Canada.

[44] Jiang, J., Xu, X., and Stringer, J., 2018, "Support Structures for Additive Manufacturing: A Review," JMMP, **2**(4), p. 64.

[45] Thomas, D., and Gilbert, S., 2014, *Costs and Cost Effectiveness of Additive Manufacturing: A Literature Review and Discussion*, 1176, NIST special publication.

[46] Kuo, Y.-H., Cheng, C.-C., Lin, Y.-S., and San, C.-H., 2018, "Support Structure Design in Additive Manufacturing Based on Topology Optimization," Struct Multidisc Optim, **57**(1), pp. 183–195.

[47] Cao, Q., Bai, Y., Zheng, Z., Zhang, J., Fuh, J. Y. H., and Wang, H., 2022, "Support Removal on Thin-Walled Parts Produced by Laser Powder Bed Fusion," 3D Printing and Additive Manufacturing.

[48] Miki, T., and Nishiwaki, S., 2022, "Topology Optimization of the Support Structure for Heat Dissipation in Additive Manufacturing," Finite Elements in Analysis and Design, **203**, p. 103708.

[49] Malekipour, E., Tovar, A., and El-Mounayri, H., 2018, "Heat Conduction and Geometry Topology Optimization of Support Structure in Laser-Based Additive Manufacturing," *Mechanics of Additive and Advanced Manufacturing, Volume 9*, J. Wang, B. Antoun, E. Brown, W. Chen, I. Chasiotis, E. Huskins-Retzlaff, S. Kramer, and P.R. Thakre, eds., Springer International Publishing, Cham, pp. 17–27.

[50] Hassani, B., and Hinton, E., 1998, "A Review of Homogenization and Topology Optimization I—Homogenization Theory for Media with Periodic Structure," Computers & Structures, **69**(6), pp. 707–717.

[51] Zeng, K., Pal, D., Teng, C., and Stucker, B. E., 2015, "Evaluations of Effective Thermal Conductivity of Support Structures in Selective Laser Melting," Additive Manufacturing, **6**, pp. 67–73.

[52] Xiaohui, J., Chunbo, Y., Honglan, G., Shan, G., and Yong, Z., 2022, "Effect of Supporting Structure Design on Residual Stresses in Selective Laser Melting of AlSi10Mg," Int J Adv Manuf Technol, **118**(5–6), pp. 1597–1608.

[53] Holmberg, E., Torstenfelt, B., and Klarbring, A., 2013, "Stress Constrained Topology Optimization," Struct Multidisc Optim, **48**(1), pp. 33–47.

[54] Liang, X., Cheng, L., Chen, Q., Yang, Q., and To, A. C., 2018, "A Modified Method for Estimating Inherent Strains from Detailed Process Simulation for Fast Residual Distortion Prediction of Single-Walled Structures Fabricated by Directed Energy Deposition," Additive Manufacturing, **23**, pp. 471–486.

[55] Sulaiman, S., Hamouda, A. M. S., Abedin, S., and Osman, M. R., 2000, "Simulation of Metal Filling Progress during the Casting Process," Journal of Materials Processing Technology, **100**(1), pp. 224–229.

[56] "A Modified Method for Estimating Inherent Strains from Detailed Process Simulation for Fast Residual Distortion Prediction of Single-Walled Structures Fabricated by Directed Energy Deposition - ScienceDirect" [Online]. Available: https://www.sciencedirect.com/science/article/pii/S2214860418304858. [Accessed: 07-Jun-2023].

[57] Cheng, L., Bai, J., and To, A. C., 2019, "Functionally Graded Lattice Structure Topology Optimization for the Design of Additive Manufactured Components with Stress Constraints," Computer Methods in Applied Mechanics and Engineering, **344**, pp. 334–359.

[58] Zipay, J. J., Modlin, C. T., and Larsen, C. E., 2016, "The Ultimate Factor of Safety for Aircraft and Spacecraft - Its History, Applications and Misconceptions," *57th AIAA/ASCE/AHS/ASC Structures, Structural Dynamics, and Materials Conference*, American Institute of Aeronautics and Astronautics, San Diego, California, USA.

[59] Shaikh, A. S., Schulz, F., Minet-Lallemand, K., and Hryha, E., 2021, "Microstructure and Mechanical Properties of Haynes 282 Superalloy Produced by Laser Powder Bed Fusion," Materials Today Communications, **26**, p. 102038.

[60] Ealy, B., Calderon, L., Wang, W., Valentin, R., Mingareev, I., Richardson, M., and Kapat, J., 2017, "Characterization of Laser Additive Manufacturing-Fabricated Porous Superalloys for Turbine Components," Journal of Engineering for Gas Turbines and Power, **139**(102102).

[61] Miki, T., and Yamada, T., 2021, "Topology Optimization Considering the Distortion in Additive Manufacturing," Finite Elements in Analysis and Design, **193**, p. 103558.

[62] Setien, I., Chiumenti, M., van der Veen, S., San Sebastian, M., Garciandía, F., and Echeverría, A., 2019, "Empirical Methodology to Determine Inherent Strains in Additive Manufacturing," Computers & Mathematics with Applications, **78**(7), pp. 2282–2295.

[63] Vaidya, R., and Anand, S., 2016, "Optimum Support Structure Generation for Additive Manufacturing Using Unit Cell Structures and Support Removal Constraint," Procedia Manufacturing, **5**, pp. 1043–1059.